

Sodium Dodecyl Sulfate-Freeze-Fracture Immunolabeling of Gap Junctions

Irene Dunia, Michel Recouvreur, Pierre Nicolas, Nalin M. Kumar, Hans Bloemendal, and E. Lucio Benedetti

1. Introduction

By the mid 1960s, pioneering work using high-resolution electron microscopy, new fixation methods, and negative staining of isolated liver plasma membranes allowed the identification of a geometric subunit pattern likely associated with junctional domains (**1,2**). Furthermore, the application of tissue impregnation with electron-dense tracers revealed that the minute “gap” (2 nm wide) between the closely adjoining junctional membranes comprised an hexagonal subunit pattern. This type of membrane–membrane interaction, distinct from tight junctions, adhesion plaques, and desmosomes, was originally called “gap junction” (**3**).

The connexins are the polypeptides forming the six subunits of a single communicating oligomer (connexon) (**4–6**). A large number of connexin isoforms has been sequenced, and several experiments have shown that the gap junction assembly even in one single tissue may display a great variety of expression patterns and that a single communicating channel may be formed by different connexin subunits (**4,5,7**). Furthermore, the gap junction phenotype is not a static character. During growth, differentiation, and aging the communicating junctional constituents are submitted to many structural and biochemical events such as phosphorylation, proteolysis, assembly, disassembly, and crystallization (**4**). Significant advances in gap junction structural biology have been achieved by a new technological endeavor. Among the novel techniques, freeze-fracture and freeze–etching have opened new avenues for the study of the fine structure of gap junctions and their modulation with developmental, functional, and biochemical events (*cf.* **ref. 8**). These techniques produced the

From: *Methods in Molecular Biology*, vol. 154: *Connexin Methods and Protocols*
Edited by: R. Bruzzone and C. Giaume © Humana Press Inc., Totowa, NJ

most solid and direct evidence of the *en face* view of the subunit organization of the junctional membranes (see **Notes 1** and **2**).

In the gap junction a pair of hexameric units, matching one another in perfect register, forms the connecting transmembrane device spanning the lipid bilayers (**4**). The freeze–fracture simultaneously splits the two opposite junctional membranes in a stepwise fashion. The cleavage passes along one of the bilayers and exposes the inner aspect of the leaflet adjacent to the cytoplasm (protoplasmic fracture face or PF), then the adjacent membrane is cleaved and the exposed fracture face corresponds to the inwardly directed face of the outer membrane leaflet (exoplasmic fracture face or EF). The junctional PF is characterized by a polygonal assembly of 9-nm intramembranous particles (IMPs). The corresponding EF displays a complementary arrangement of pits or depressions (**9,10**) (see **Note 2**). However, conventional freeze–fracture and etching do not provide information on the chemical nature of the pleiomorphic features of the gap junctions visualized on the fracture faces. This inherent limitation of the technique prompted several investigators to develop new methods combining freeze–fracture and etching with immunocytochemical labeling. The aim of such technological development was to study in parallel the ultrastructural features and the biochemical nature of the membrane constituents (**11–14**). Among the different methods of immunolabeling, the sodium dodecyl sulfate-digested freeze–fracture replica labeling (SDS-FL), originally developed by Fujimoto (**15**), produced consistent information on the organization of the intercellular junctions, particularly during their assembly and functional changes (**Fig. 1**, see **Note 3**).

The basic principle of the SDS-FL technique is that the freeze-cleaved membrane halves become physically stabilized by the metal shadowing during replication. These stabilized membrane halves are not dissolved by the detergent, as the apolar inner membrane core positioned against and stabilized by the metal cast became resistant to detergent solubilization. The detergent treatment, however, may unravel and/or expose antigenic polar domains anchored to the stabilized membrane structure and allow immunolabeling thereafter (**Fig. 2**, see **Note 4**). A recent modification of SDS-FL, using Lexan stabilized freeze–fracture replicas, has been proposed by Rash and Yasumura (**15a**).

2. Materials

2.1. Quick Freezing

1. A Dewar flask filled with liquid nitrogen (Balzers, Liechtenstein).
2. A solid metal cylinder comprising a small receptacle at the top (3 cm depth), sitting across the neck of the Dewar flask (Balzers).
3. Propane gas bottle (Balzers) and regulator valve to control the flow of gas coming out (see **Note 5**).

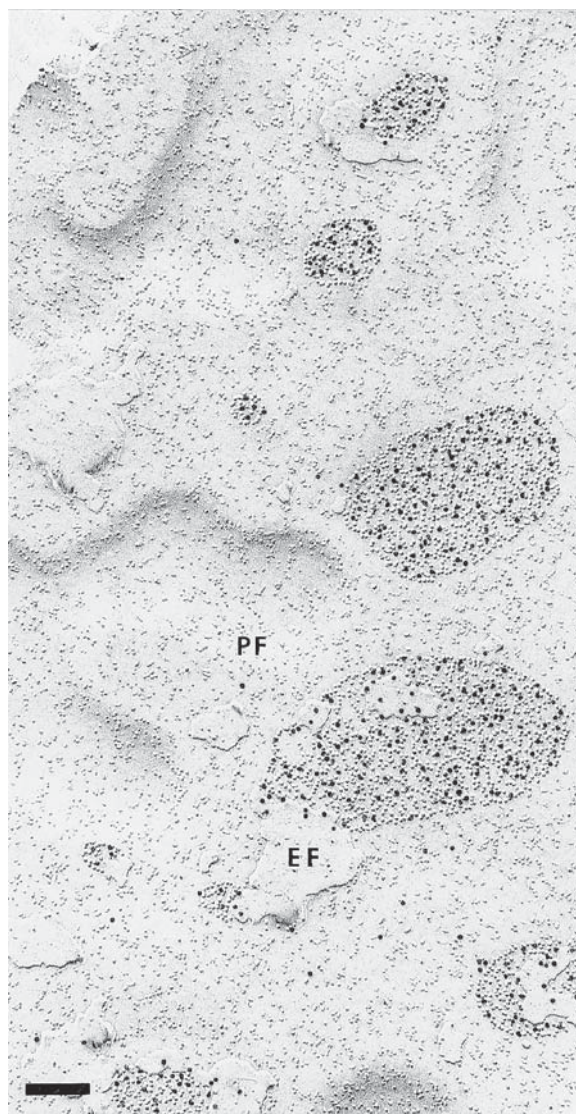


Fig. 1. SDS-FL of the outer lens cortex where the assembly of gap junctions connecting the elongating fibers takes place. Immunogold labeling (10-nm gold particles) using the polyclonal antibody directed against the middle cytoplasmic domain of Cx50, between the second and third transmembrane domains. Freeze-fracture has mainly exposed the membrane leaflet close to the cytoplasm, protoplasmic fracture face (PF). Only small fragments of the exoplasmic fracture face (EF) are exposed. Note the great variety in size of the newly assembled junctional domains, characterized by clusters of identical 9-nm intramembrane particles (IMPs). The immunogold labeling is specifically restricted to the junctional plaques. Bar = 80 nm.

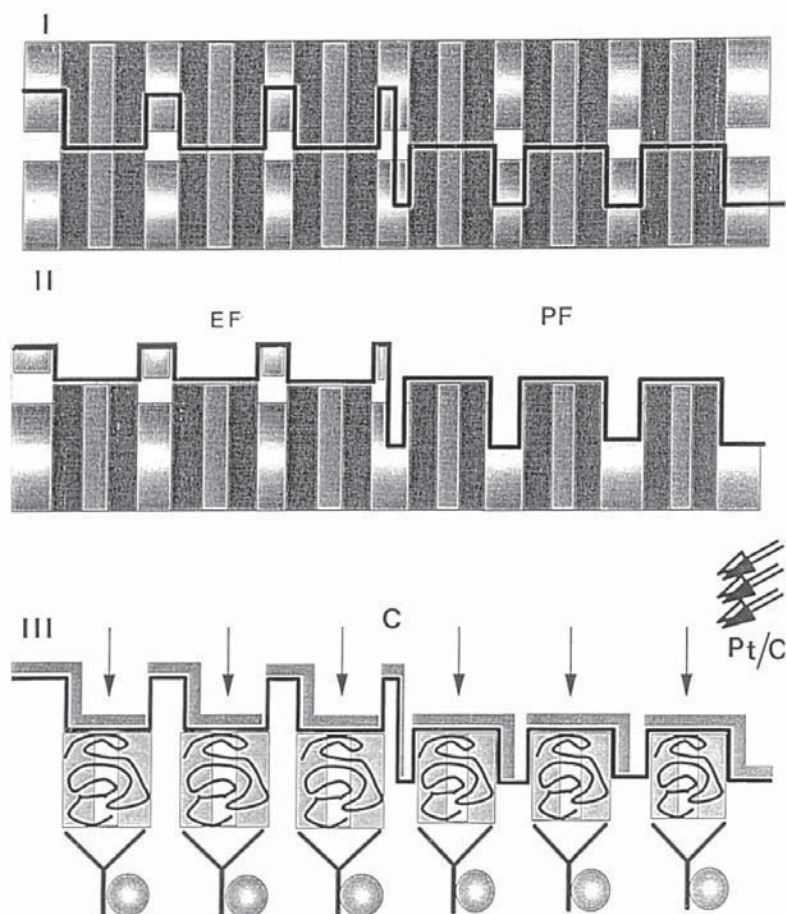


Fig. 2. Diagrammatic representation of the SDS-FL of gap junctions. At low temperature (-150°C) the cleavage plane splits the junctional membranes into two halves, exposing both the pitted exoplasmic fracture face (EF) and the protoplasmic fracture face (PF) where the single connexons are anchored (I and II). SDS solubilization unravels the antigenic sites of connexins exposed at the cytoplasmic surface of the junctional membrane (III). Both fractured and uncleaved junctional bilayers are hold and remain “stabilized “ by the platinum/carbon replica (Pt/C and C), allowing the subsequent gold immunolabeling (III).

4. Another Dewar flask filled with liquid nitrogen to store specimens after freezing.
5. Specimen holders: precleaned gold–nickel alloy discs with a central solid flat-topped platform (Balzers), previously scratched lightly in a criss-cross pattern with a scalpel blade, to increase the adhesion of the frozen sample.
6. Fine-tipped forceps.

2.2. Freeze-Fracture and Replication

1. A freeze-fracture apparatus, model 301 or 400 (Balzers), equipped with a turbomolecular pump, liquid nitrogen-cooled trap and electron gun beams ready to evaporate: a platinum and a carbon layer (Pt/C) at an oblique angle of about 45° and a perpendicular layer of carbon respectively.
2. Quartz crystal thin film monitor (Balzers).
3. Appropriate styrofoam box filled with liquid nitrogen to cool the specimen holder injector.
4. Precision tweezers.

2.3. Detergent Treatment of the Replica

1. Phosphate-buffered saline (PBS), pH 7.4.
2. Buffered 2% SDS in 10 mM Tris-HCl and 30 mM sucrose, pH 8.3.
3. Porcelain spotting plaques.

2.4. Immunolabeling

1. PBS, pH 7.4.
2. 1% Bovine serum albumin (BSA) in PBS.
3. 0.2% BSA in PBS.
4. 0.5% Glutaraldehyde in PBS.
5. 50 mM Glycine in PBS.
6. Reagents were obtained from Sigma, unless otherwise indicated.

2.5. Antibodies

1. Affinity-purified rabbit polyclonal antibodies directed against the major intrinsic membrane protein of the lens fibers (MP26) that recognize the native protein (**16**) at a 1:500 dilution.
2. Rabbit polyclonal antibodies directed against MP26 that recognize the native protein and its proteolytic derivatives (**17**) at 1:200.
3. Affinity-purified polyclonal antibodies directed against the Cx46 J peptide (**18**) (see **Subheading 3.5., step 3**) at 1:200.
4. Polyclonal antibodies directed against a Cx50 peptide (**19**) at 1:200 dilution.
5. Monoclonal antibody directed against MP70 (Cx50) (**20**) at 1:200 dilution.
6. Protein A conjugated to 15- or 10-nm gold particles (Department of Cell Biology, University of Utrecht, The Netherlands).
7. Mouse-IgG coupled to 15- or 10-nm colloidal gold particles (Amersham).

2.6. Mounting the Replica

1. Distilled water.
2. 300-mesh coated (thin film of Formvar or collodion) grids for electron microscopy.
3. 0.3% Formvar solution (dichloroethane) or 1% collodion (chloroform).
4. Precision tweezers.

3. Methods

3.1. Dissection and Preparation of the Frozen Specimens

1. The Dewar flask filled with liquid nitrogen is placed in the fume cupboard; the solid metal cylinder, comprising a small receptacle at the top, is placed inside. Propane from the bottle is dispensed into the inner receptacle with the regulator valve adjusted to give a slow flow to fill it completely with condensed propane.
2. The material to prepare the samples has to be dissected immediately after the animals are killed. Very small (0.25 mm^3) and thin pieces of the biological material were placed on the specimen holders under a binocular microscope.
3. Once the propane was cooled to -180°C (*see Note 5*), each mounted specimen held in a fine-tipped forceps was manually plunged into the liquid propane, at the highest speed possible. The specimens need to be made and frozen one by one (working temperature about 93 K or -170°C), to avoid drying and shrinkage of the sample. After standing each sample in the liquid propane for about 15 s to rapidly freeze it, the samples need to be rapidly transferred into the liquid nitrogen contained in the second Dewar flask to store them (*see Note 6*). The opening of the propane receptacle must be kept covered with a polystyrene lid between freezing runs.

3.2. Freeze-Fracture and Replication

1. Start the pumping procedure of the freeze–fracture unit once the electron beam guns are ready and the knife (razor blade) of the microtome arm has been changed.
2. Preheat the electron beam guns when vacuum is 10^{-5} Torr. Pt/C gun: 1000 V , 50 mA , preheating for 2 min . C gun: 1500 V , 50 mA , preheating for 5 min .
3. Start the cooling process of the specimen table to -150°C (about 15 min) and the cooling of the microtome arm.
4. Start to cool the injector and the specimen holder plate by immersion in the adapted styrofoam box.
5. Transfer carefully, with a precooled tweezers, one sample (stored in liquid nitrogen) to the precooled specimen holder plate in the liquid nitrogen.
6. When the specimen table is cold (-150°C), open the trap of the freeze–fracture unit adapted for introducing the injector holding the specimen.
7. Take out the injector and close the trap as soon as the sample is well fixed in the specimen table.
8. When the microtome arm is cold (-196°C) and the vacuum reaches at least 5×10^{-7} Torr (about 20 min after replacement of the sample), adjust at -140°C the temperature of the sample table (requires approx 10 min).
9. Wait till the vacuum is 2×10^{-7} Torr.
10. Fracture the specimen superficially with great care, moving the cold microtome arm and “fracturing” the surface of the specimen with the cold knife. Carefully control these manipulations through the binocular stereo microscope outside the vacuum chamber (*see Note 7*).

11. Cover the final fractured surface of the specimen by placing the microtome arm above the sample as soon as the fracture is completed.
12. Start the heating of the electron gun beam for Pt/C evaporation. As soon as the appropriate current values are 1900 V and 90 mA, the evaporation on the specimen can start: uncover the fractured surface, by moving away the microtome arm, and shadowcast the specimen with a 2 nm Pt/C evaporation at an oblique angle of 45°, controlling the thickness of the Pt/C deposit on the quartz crystal monitor.
13. Switch off the Pt/C evaporation and switch on the electron gun beam for carbon at 2300 V and 120 mA. Evaporate a perpendicular 20-nm carbon layer (*see Note 8*).

3.3. Thawing and Detergent Treatment

1. Once the replication process has been completed, the trap is vented and the specimen holder is removed with the injector.
2. Manipulate the specimen holder carefully with tweezers. Thawing of the replica should be very delicately achieved to minimize fragmentation. Use a stereomicroscope to control the different manipulations.
3. The replica is detached from the tissue by immersion in PBS, with gentle agitation, using a plastic pipet, to create a movement of the surrounding liquid around the replica. Porcelain spotting plaques are used for all manipulations.
4. As soon as the replicas, complete or in pieces, are detached from the bulk of the biological material, they are transferred to 2% SDS–Tris–sucrose buffer, taking care to immerse the replica completely in the detergent solution. Intermittent agitation, with a plastic pipet, is produced. Change the SDS solution 3–4 times. The total SDS treatment is prolonged for 1–2 h maximum (*see Note 4*).
5. Next, wash the replica thoroughly in PBS (6 × 3 min).

3.4. Immunolabeling

3.4.1. Simple Immunolabeling

1. To saturate nonspecific binding sites, incubate in PBS–1% BSA for 10 min.
2. Incubate with a specific antibody at an appropriate dilution in PBS–0.2% BSA for 30 min.
3. Wash 5×, 3 min each, in PBS–0.2% BSA.
4. Incubate with protein A–gold at an appropriate dilution or with the corresponding gold-labeled IgG diluted in PBS–0.2% BSA for 20 min.
5. Wash 5× in PBS, 3 min each.
6. Fix in 0.5% glutaraldehyde in PBS for 5 min.
7. Wash several times in distilled water before mounting the replica on grids previously covered with a thin film of Formvar or collodion.

3.4.2. Double Immunolabeling

1. Incubate in PBS–50 mM glycine (2 × 5 min).
2. Glycine is used to quench free aldehyde groups.

3. For double or triple labeling, repeat all the steps of simple immunolabeling, either once (double labeling) or twice (triple labeling) (*see* **Notes 9–11**).

3.5. Antibodies Raised Against Connexins and MP26

3.5.1. Polyclonal Antibodies

1. Antiserum directed against MIP. Rabbit antiserum purified SDS-denatured calf MIP (MP26) was prepared as described previously (**21**). Lens membranes enriched in junctions were solubilized in SDS, reduced, alkylated, and separated on preparative SDS gels. Gel strips corresponding to proteins with a molecular mass of approx 26 kDa were removed from the preparative gel and crushed. Immunization was done by injection of the crushed gel strips in complete Freund's adjuvant. The resulting antiserum recognized a single component in lens membranes with a molecular mass of 25.5 kDa—MIP—from calf, mouse, rat and chicken by Western blotting and by immunohistochemistry on frozen sections (**16,21**), and did not recognize lower molecular weight, presumably degraded forms, of MIP. The antiserum against MIP was used at 1:500 for immunofluorescence and SDS-FL.
2. Antiserum directed against MP26. This antiserum was produced in rabbits against a chloroform–methanol extract of MP26 (**22**), solubilized from isolated lens fiber plasma membranes, as described (**23**). The resulting antiserum specifically recognized MP26 and its degradation products (MP22, lower molecular weight) by immunoblotting (**17**). The antiserum against MP26 was used at 1:200 dilution for SDS-FL.
3. Antibody directed against a Cx46 (Cx α 3) J peptide. Cx α 3J peptide corresponds to the intracellular loop (J) based on the putative topology of connexins (**24**) and the amino acid sequence of rat Cx46 (**25**). This peptide was synthesized with a cysteine added to the C-terminus to facilitate attachment to a carrier protein, KLH (keyhole limpet hemocyanin). The sequence of the peptide was as follows: RRDNPQHGRGREPMC, assigned to residue 115–128. The synthetic peptide was coupled to KLH using *m*-maleimidobenzoyl-*N*-hydroxysuccinimide ester (MBS) as previously described (**24,25**). The generation of polyclonal peptide antiserum in rabbits was carried out as previously described (**24,25**). The Cx46 antibodies were affinity purified and characterized by Western blotting and immunofluorescence analysis (**18,26–28**). By these criteria, this antiserum recognizes the full-length form (44.6 kDa) of Cx46, as well as smaller degradation products, but does not cross-react with other connexins. The Cx α 3J antiserum was used at a 1:200 dilution for immunohistochemistry and SDS-FL.
4. Antibody directed against a Cx50 peptide. This antiserum was produced in rabbits against a synthetic peptide corresponding to residues 124–136 of Cx50 as described in **ref. 19**. The Cx50 antiserum was characterized by Western blotting and immunofluorescence analysis (**19**). We used a 1:200 dilution of this antiserum for SDS-FL.

3.5.2. Monoclonal Antibodies

1. Antibody to Cx50 (6–4 B2-C6). A mouse monoclonal antibody to Cx50 was generated using urea-extracted membranes isolated from sheep lenses (20). Antibodies from the hybridoma cell line (6–4 B2-C6) were found to be specific for fiber membrane junctional domains as determined by Western blotting and immunohistochemistry (20,29). Hybridoma 6–4 B2-C6 recognizes antigens present in calf, chicken, mouse, rat, and toad (20). Cleavage of Cx50 to a 38-kDa form resulted in a loss of the epitope recognized by this monoclonal antibody (30). Hence, this antibody is likely to recognize a c-terminal domain (31). This monoclonal antibody was used at a 1:200 dilution for immunohistochemistry and SDS-FL.

3.6. Mounting the Replica

This procedure is the final step before the examination of the SDS-FL in the electron microscope. Once the immunostaining is achieved, and after several washes in distilled water where the replicas have been completely immersed, it is necessary to float them at a clean surface of distilled water. Floating replicas may be mounted on electron microscopy grids (Formvar-coated or collodium-coated grids) from above or below, depending on the individual's preference. As cleaning, mounting is always carried out with the aid of a binocular microscope. When mounting from above is done, the grid, held by the tips of fine forceps, is brought face-on into contact with the replica, pushing it down into water, and then, in a single continuous twisting movement, the grid is turned over and out of the water, carrying the replica on top. Any traces of water are carefully removed with pointed strips of filter paper applied to the edge of the grid. Freeze-fracture replicas are chemically inert and reasonably resistant to damage by electron irradiation. If stored in a clean environment replicas will last indefinitely. The resolution of a replica is limited by the dimensions of the metal grains used to generate contrast, being 1.5–2 nm for a Pt/C replica.

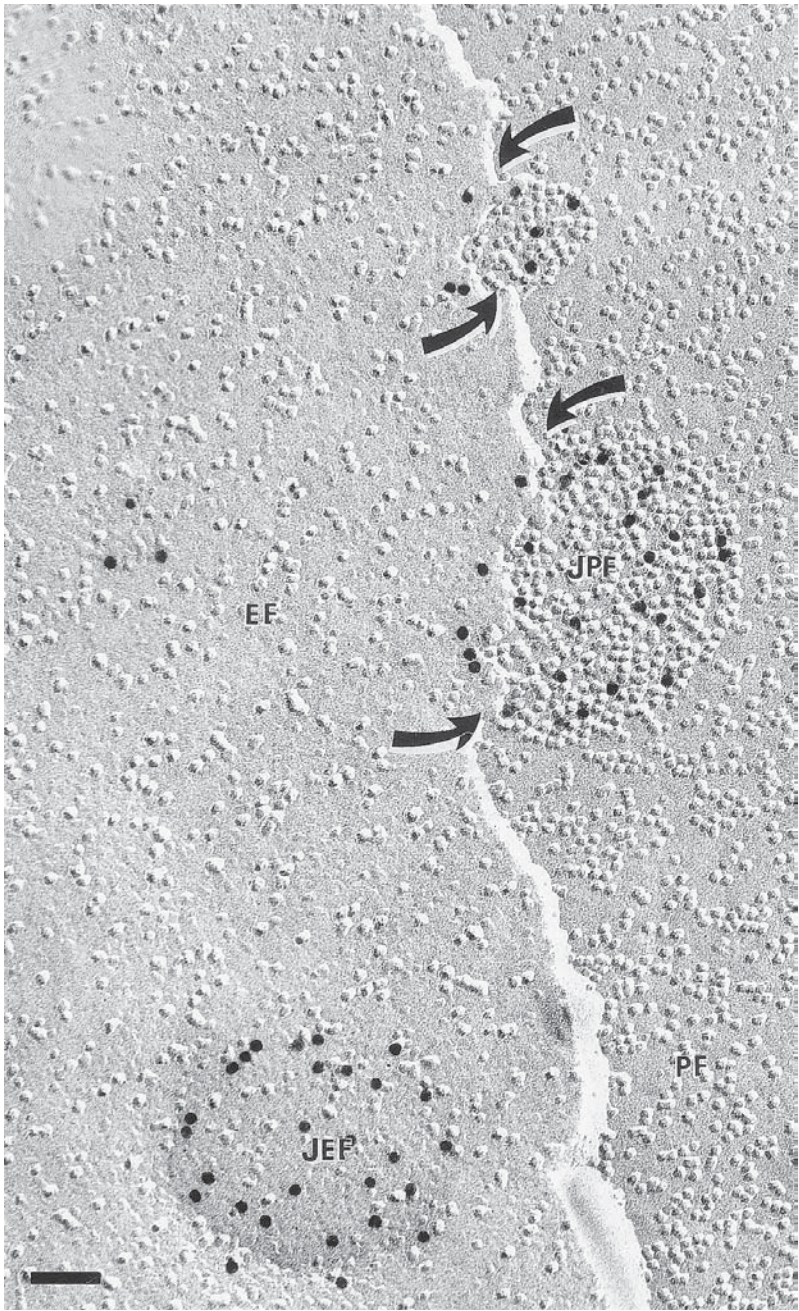
4. Notes

1. During freeze-fracture the membrane bilayer is cleaved along its hydrophobic core. Thus the freeze-fracture reveals the internal organization of both the lipid and the protein of the inner core of the membrane bilayer. In addition, freeze-etching exposes the ultrastructural features of the true external and inner cytoplasmic surfaces of the membranes. Therefore, the observation of both fractured and etched exposed faces provide a tridimensional view of the membrane (32–35; cf. refs. in 36). In a replica of a biological membrane, the inner protoplasmic face (PF) of the leaflet cleaved along its hydrophobic matrix shows a heterogeneous appearance characterized by smooth areas and particulate entities ranging in diameter from 4 to 14 nm (intramembranous particles or [IMPs]) likely comprising the transmembrane proteins. The exoplasmic fracture face (EF) is

characterized by the presence of few IMPs and multiple small pits created by the transmembrane proteins dislocated from the outer half of the bilayer. Thus a distinct asymmetric distribution of IMP is found in freeze-fractured biological membranes. The transmembrane proteins interact more strongly with the protoplasmic half of the bilayer (PF) and/or with extrinsic constituents associated with the inner cytoplasmic surface of the membrane (37). The IMP partition coefficient (K_p) between PF and EF can be calculated as follows: $K_p = CP/CE$, where CP and CE are the concentrations in number of IMPs per unit surface adhering to the PF and to the EF, respectively. During freeze-fracture, integral membrane proteins are asymmetrically partitioned between EF and PF. Therefore, each resulting cleaved membrane half does not contain the entire set of proteins, and probably of lipids, present in the intact membrane (38). So far, it is not easily apparent whether or not connexons, built up by a distinct set of connexins, have a preferential partition coefficient for either PF or EF. The application of SDS-FL using site-directed antibodies will be a useful tool for addressing the preferential partition of connexin isoforms (*cf.* ref. 24).

2. We anticipated that in the gap junction the fracture plane extends from one to the other membrane of the same junction. Thus, freeze-fracture of junctional membranes splits the hydrophobic interior of each bilayer, exposing IMPs on the protoplasmic leaflet (JPF) and their complementary pits on the exoplasmic leaflet (JEF). Obviously, junctional IMPs comprise connexins (Figs. 3 and 4). It might also be that junctional IMP enclosed not only connexins but also tightly bound lipids and auxiliary proteins (39). These remarks should be taken into consideration when one needs to elucidate the results of the SDS-FL experiments. Another interesting problem concerns the region where the connexon pairs are fractured. Experiments carried out with high-resolution rotary shadowing have provided the evidence that the junctional particles on PF may display different heights (40). This observation suggests that the freeze-fracture of connexon pairs takes place randomly and even along protein domains with prevailing covalent bonding (37,38). We should, however, take into consideration that other data obtained by rapid freezing (41), atomic force microscopy (42), and three-dimensional electron crystallography (43–45), of split or recombinant gap junction membranes demonstrated that the connexon-exposed outer surface is characterized by struc-

Fig. 3. SDS-FL of the outer lens cortex using polyclonal antibodies raised against the cytoplasmic exposed Cx50 domain. The freeze-fracture has simultaneously split the opposite bilayers of two adjoining lens fibers. The cleavage opened the inner core of one bilayer and exposed the exoplasmic fracture face (EF). Then, the fracture passed in a step-by-step fashion along the bilayer of the adjoining plasma membrane and discovered the inner aspect of the protoplasmic fracture face (PF). One junctional plaque can be identified on EF by the presence of a round-shaped agglomeration of small depressions (JEF). The gold immunolabeling is positively associated with the pitted plaque. The two junctional plaques exposed on PF, (JPF) are characterized by the assembly of 9-nm intramembrane particles (IMPs). The gold immunolabeling is



restricted to the junctional domains. The *arrows* point to the sites where the intercellular gap is abruptly reduced. Bar = 50 nm.

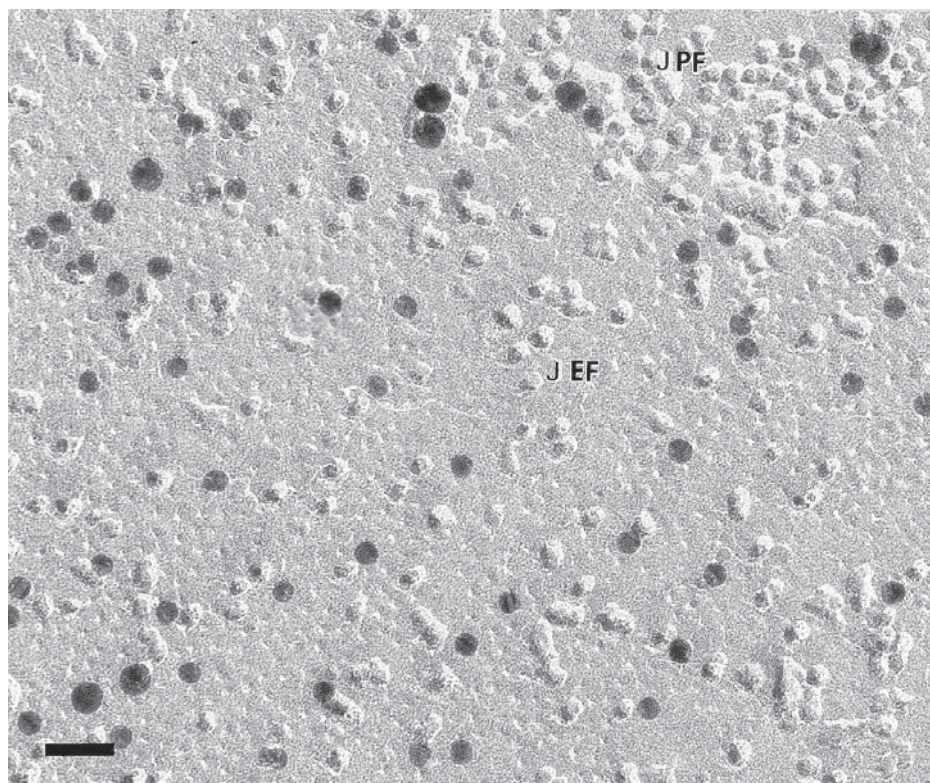
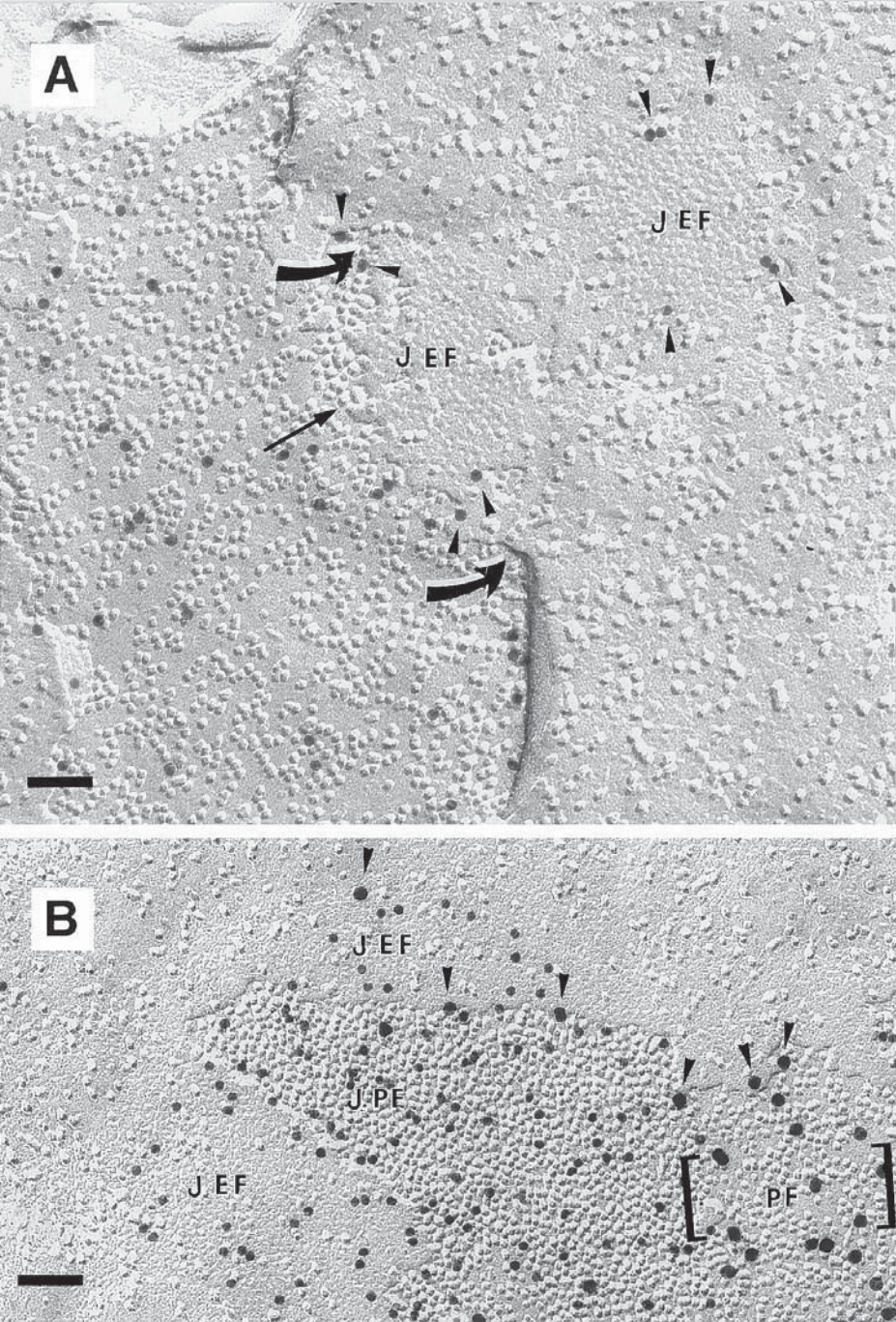


Fig. 4. SDS-FL of cortical lens fiber plasma membranes. Double-immunolabeling with antibodies directed against Cx46 (15-nm gold particles) and Cx50 (10-nm gold particles). The double labeling shows that these two lens connexins are codistributed on the same junctional plaque. JEF, junctional exoplasmic face; JPF, junctional proto-plasmic face. Bar = 40 nm. Reproduced from Dunia et al. (55).

tural features comparable to junctional IMPs on PF of conventional replicas of intact gap junctions. These observations suggest that the IMPs visualized on PF of gap junctions are primarily single connexons exposed by a freeze-fracture plane that passes in the middle of the extracellular docking domain of connexon pairs. The proposed freeze-fracture mechanism of the gap junction and the results of SDS-FL will be better understood if one takes into consideration the molecular model illustrating the vertical interaction of the connexins forming the transmembrane communicating pair. A model conceives that the two extracellular loops (E1 and E2) of each connexin connected by disulfide bonds (46), forming a hemichannel dock with the opposite connexin-exposed segments and interdigitates like the two sides of a “zip.” The extracellular loop region consists of stacked intercalated β -sheets resulting in an antiparallel β -barrel motif. The bar-

rel would possess concentric layers, one formed by E1 loops and the other by E2 loops, respectively. The outer surface and the center of the barrel are essentially hydrophilic. Conversely, the interphase between the two concentric layers is expected to be highly apolar, composed mainly of intercalated hydrophobic side-chains of residues originating from two opposed β -sheets (44–48). Such a tightly packed hydrophobic wall should confer high stability to the docking of the two connexons forming a pair. It may also explain why conditions used for splitting the gap junctions are usually chemically harsh, involving alkaline pH, chaotropic agents (urea), or a combination of the two treatments (41,42,48,49; for additional references see Chapter 3 by Sosinsky and Perkins in *this volume*). Furthermore, the molecular features of the docking domain of the connexon pairs will constitute a barrier preventing any leakage from inside the channel to the extracellular space (gap). On the other hand, during freeze-fracture the extracellular domain will be the most fragile site of the connexon pair because at low temperature the hydrophobic bonds are weakened. Therefore, the extracellular domain between two opposed connexons represents the site where the freeze-cleavage can abruptly disjoin the connexon pair (Fig. 2).

3. The application of SDS-FL is very useful for the study of the relationship between connexin assembly and cell surface proteins that are implicated in cell–cell recognition and membrane–membrane interactions (50–53). SDS-FL will also contribute to the definition of the close lipid environment in the gap junction domains by using specific antibodies against the lipid moiety of the membrane (54). In addition, SDS-FL could provide some clues on the potential role of the major intrinsic lens fiber membrane polypeptide (MP26) during gap junction assembly (55). This event occurs during the terminal differentiation of epithelial lens cells into elongating fibers (56). The results of SDS-FL suggest that MP26 forms transmembrane oligomers randomly distributed in the general plasma membrane that upon freeze-fracture remain anchored to the PF (Fig. 5), likely functioning as aquaporin (57). On the other hand, MP26 oligomers may also constitute around the gap junctional domain a borderline of transmembrane linked pairs according a model purported for connexon pairs (see Note 2 and ref. 55). Hence the application of SDS-FL suggests that a membrane constituent—MP26—may fulfill different functions and is integrated within the lipid bilayer in different conformations (Figs. 5 and 6). Furthermore the SDS-FL is a method of general applicability for the identification of spatial distribution of constituents that are involved in the assembly of specialized plasma membrane domains (desmosomes, tight junctions, etc.), and immunochemically characterize the extrinsic membrane proteins that are implicated in cell surface modulation (58,59).
4. The assumption of Fujimoto (15), addressing the feasibility of SDS-FL, is that the freeze-cleaved membrane halves on the metal shadowing somehow became grasped by the Pt/C mold and physically stabilized. As a consequence the apolar inner core of the cleaved membrane halves are no longer accessible to the SDS binding. Nevertheless, SDS treatment may extract extrinsic membrane constituents and unravel connexon antigenic sites associated with the “stabilized” proto-



plasmic fracture (PF) halves. The immunolabeling will be further facilitated by washing out the detergent with PBS. An important question concerns the mechanism of gold immunolabeling of the pitted junctional exoplasmic fracture (EF) faces. This question is especially pertinent when the antibody used for immunolabeling recognizes connexin antigenic sites exposed at the cytoplasmic surface of the junctional membrane. One should consider the fact that proteins differ in their intrinsic stability toward SDS solubilization. There exist several examples of protein–lipid membrane domains resistant to SDS denaturation and that may form complexes with the SDS (60–62). Therefore one hypothesis could be that the tight protein–protein and protein–lipid interactions between connexons are relatively stable toward the detergent treatment applied for SDS-FL and that SDS instead of denature may promote formation of complexes (63,64). At this point, it is also noteworthy to recall that gap junctions were originally isolated from the general plasma membrane because this specialized domain is resistant to detergent solubilization (65,66). Hence the stability of the gap junction protein–lipid scaffold toward detergent treatment during SDS-FL likely accounts for the persistent association between the connexons within the uncleaved junctional membrane and the freeze-fractured and replicated membrane halves recognized as junctional pitted EF (**Fig. 2**). We assume that the evidence of gold particles apparently labeling the junctional EF in fact correlates with the gold immunolabeling of the cytoplasmic exposed antigenic sites of connexin within the uncleaved bilayer.

5. Extreme care must always be taken to eliminate any possibility of an explosion hazard when working with liquefied flammable gases in general and particularly with propane. All work must be undertaken within the confines of an extraction fume cupboard suitable for allowing safe escape of flammable vapors and naked flames. Electrical switches that might generate sparks must be excluded from the work area. The liquefied cryogen should be safely discarded after each experi-

Fig. 5. (Opposite page) (A) SDS-FL of cortical lens fibers plasma membranes using polyclonal antibodies raised against MP26 (10-nm gold particles). Both junctional protoplasmic (PF) and exoplasmic faces (EF) are exposed. MP26 immunolabeling remains almost exclusively associated with PF. Conversely, MP26 immunolabeling of EF specifically delimits the borderline between the junctional domain and the general plasma membranes (*arrowheads*). *Curved arrows* point to the site where the intercellular space is reduced. *Black arrows* point to the accumulation of junctional intramembrane particles (IMPs) on PF. **(B)** SDS-fracture double-immunolabeling of cortical fiber plasma membrane with anti-MP26 (15-nm gold particles) and anti-(Cx50 (10-nm gold particles). The immunolabeling of anti-Cx50 (10-nm gold particles) is specifically localized where arrays of 9-nm identical IMPs are closely packed. Conversely, MP26 immunolabeling (15-nm gold particles), is mainly confined to areas where IMPs on PF are randomly distributed (bracket) or along the rim between EF and PF where the intercellular space is reduced (*arrowheads*). Bars = 50 nm.



Fig. 6. SDS-FL of cortical lens fibers plasma membrane using polyclonal antibodies raised against MP26. The freeze-fracture exposes a large EF surface. The junctional plaque (JEF) appears as a round-shaped pitted depression. The gold immunolabeling is positively restricted to a belt surrounding the junctional domain (*arrowheads, brackets*). Bar = 50 nm.

ment, either by evaporation within the fume cupboard or by carefully pouring the liquid onto the ground at a distance from people, automobiles, and buildings and other installations.

6. The preparation of the frozen specimens to be fractured and replicated is a crucial step of this technique. The routine method of overcoming the problem of damaging ice crystal formation is the use of a cryoprotectant, with or without previous chemical fixation. For SDS-FL because the material has to be processed unfixed the critical freezing rate of the specimen should be increased to ensure best freezing, to reduce the size of ice crystals compatible with the induction of the so-called vitrification state of the biological specimen. The first sections from the surface of the specimen (measuring 5–20 μm) are properly and quickly frozen. In this “vitrified” state the amount and distribution of the water content of the specimen are preserved. The specimen should be as small as possible and the time interval between sampling and freezing of each sample should be as short as possible to avoid modifications of the structure. Many rapid-freezing methods exist: high-pressure freezing, spray freezing, jet freezing, plunge freezing, and cold-block freezing. The results are satisfactory but they often involve sophisticated and expensive equipment. The entry velocity attainable by manual plunge freezing is not as high or as reproducible as can be achieved using a mechanical device, but the method is simple, has negligible cost, and, with practice, gives consistently good results when used with thin specimens. The detailed methodology, advantages and disadvantages of different techniques are exhaustively described elsewhere (*cf.* 67,68). Once the specimens are frozen they can be used directly for further processing or stored for use at some future time. Frozen specimens must be handled in such a way that temperature increase does not occur. In particular, temperature should not be allowed to rise above about 90 K (-150°C), because some ice crystal growth may occur. Storage in liquid nitrogen is both safest and easiest, and perfectly suitable for specimens to be used for freeze-fracture replication.
7. The fracturing process cleaves the frozen specimen along the plane that offers the least resistance to the applied forces, namely, along the membrane hydrophobic core. Fracturing is done with a microtome knife edge (razor blade). The zone of ideal freezing of the specimen is limited to a thickness between of 5 and 20 μm from the surface depending on the quick-freezing method used (*cf.* 67,68). Thus, the frozen specimen should be fractured superficially.
8. Deposition of the shadowcast (replica) onto the specimen fracture faces must be done in a vacuum coating unit. Excellent vacuum conditions, with a minimum of condensable gases around the specimen during exposure of the fracture planes to the metal deposit, are essential. Several liquid nitrogen or helium-cooled traps have been developed. The aim of these devices is to surround the sample with a cold trap to avoid contamination of the specimen fracture faces particularly with water vapor condensing from either the vacuum unit or parts covered with hoar frost (*cf.* 67,68). The replication process should copy the relief produced by specimen fracturing. This process involves two steps. First, an electron-opaque metal, Pt/C, is evaporated onto the specimen at an oblique angle (approx 45°) to the

average orientation of the fracture planes to provide contrast. Second, the patches of shadowed material are bound together and reinforced by the deposition of a low electron-scattering layer of carbon evaporated perpendicular to the fracture plane. Several parameters increase shadowing resolution (*cf.* 67,68). The user of the freeze–fracture technique is often confronted with the question of whether or not the results of the application of this method are credible. We may assume that when the main physical parameters governing each step of the technique are thoroughly controlled and optimized (69), this method of specimen preparation yields reliable information almost devoid of artifacts. Nevertheless the use of comparative techniques in conjunction with freeze–fracture and etching will provide useful data that will corroborate the interpretation of the replica (*cf.* 67,68). It is noteworthy to recall that the combination of freeze–fracture and low temperature X-ray diffraction experiments has provided evidence that the crystalline order of complex lipid–water phases remains preserved after freeze–fracture and replication (70).

9. Immunolabeling needs to be performed under extremely clean conditions, with freshly prepared solutions and filtered water. It is important to always keep the replicas wet. Appropriate controls are necessary—for a single immunolabeling, using a comparable nonspecific antibody instead of the specific antibody and testing the protein A–gold conjugate alone without primary antibody. As controls for double or triple labeling, each step needs to be performed separately as a single immunolabeling. For double or triple labeling, one may ask what is the best choice of the size and the order of the gold particles. This should be tested by trial and error. In a multiple labeling procedure the yield of the later gold step is less than in a simple labeling (*cf.* 71). Thus, it is advisable to label the scarcest antigen first, using the largest size of gold particles. The best combination is found by changing the order of the different sizes of gold particles for the same kind of double or triple labeling. Can one gold particle be interpreted as a positive reaction? Any label observed has to be considered specifically if the antibody is characterized by biochemical means as giving a positive reaction. The labeling efficiency of the SDS–FL corresponds to the proportion of an antigen in a replica that is recognized by an antibody, or the number of immunogold particles divided by the known number of antigens that they label. For other methods of immunolabeling, the labeling efficiency is rarely above 10%. Thus, one gold particle can be judged as a positive reaction for an antigen present at very low amounts. Without doubt, this is a handicap for immunocytochemistry at the electron microscopy level, as only antigens present in relatively high amounts can be immunolocalized. When the background is low or nondetectable, more than three gold particles are judged as a positive reaction.
10. Several factors affect the labeling efficiency. First, experimental variables: the quality of the antibody and of the gold and several labeling parameters such as the length of the labeling, dilution of the antibody and gold, temperature, etc. Second, antigen-related variables deal with the different conformations of the antigens to be labeled. Third, the fracture mechanism, detergent treatment, and

particularly the molecular conformation of the constituent (for proteins: number of transmembrane domains, posttranslational modifications, etc.) need to be taken into account. In our experience, prolonged SDS treatment (6–12 h) diminishes the labeling efficiency. Finally, an additional factor to be considered at high antigen concentration is the possibility of steric hindrance, that is, the presence of one bound antibody and /or gold particle may hinder the access of further antibody/gold particles to closely adjacent antigens.

11. The semiquantitative evaluation of immunogold labeling can be applied to SDS-FL, including basic stereology. This methodology has been extensively reviewed (*cf.* 72–74). Quantitative estimation of the immunolabeling of connexins on the gap junction domain, respectively on PF and EF, has been thoroughly illustrated by (50) and (53).

Acknowledgments

We gratefully acknowledge the stimulating discussions and support of Pr. N. B. Gilula during our work. We wish to thank Dr. J. G. Dunia for his friendly help and expertise in computer-assisted drawing. The original studies of the authors have been supported by a Collaborative Research grant from NATO International Scientific Exchange Programs on Lens Plasma Membranes and Cataract, by the Alcon Research Institute Awards to E.L. Benedetti and H. Bloemendal, and by the French National Research Council (CNRS).

References

1. Robertson, J. D. (1963) The occurrence of a subunit pattern in the unit membrane of club endings in Mauthner cell synapses in goldfish brain. *J. Cell Biol.* **19**, 201–221.
2. Benedetti, E. L. and Emmelot, P. (1965) Electron microscopic observations on negatively stained plasma membranes isolated from rat liver. *J. Cell Biol.* **26**, 166–174.
3. Revel, J. P. and Karnovsky, M. J. (1967) Hexagonal array of subunits in intercellular junctions of the mouse heart and liver. *J. Cell Biol.* **33**, C7.
4. Kumar, N. M. and Gilula, N. B. (1996) The gap junction communication channel. *Cell* **84**, 381–388.
5. Bruzzone R., White, T. W., and Goodenough, D. A. (1996) The cellular internet: on-line with connexins. *BioEssays* **18**, 709–718.
6. Nicholson, S. and Bruzzone, R. (1997) Gap junctions: getting the message through. *Curr. Biol.* **7**, 340–344.
7. Jiang, J. X. and Goodenough, D. A. (1996) Heteromeric connexons in lens gap junction channels. *Proc. Natl. Acad. Sci. USA* **93**, 1287–1291.
8. Bennett, M. V. L. and Spray, D. C. (1985) *Gap Junctions*, Cold Spring Harbor Laboratory Press, Cold Spring Harbor, New York.
9. Staehelin, L. A. (1979) A simple guide to the evaluation of the quality of a freeze-fracture replica, in *Freeze-Fracture Methods, Artifacts, and Interpretations* (Rash, J. E. and Hudson, C. S., eds.), Raven Press, New York, pp. 11–17.

10. Peracchia, C. and Peracchia, L. L. (1988) Gap junction dynamics: reversible effect of hydrogen ions. *J. Cell Biol.* **87**, 719–727.
11. Pinto Da Silva, P., Parkison, C., and Dwyer, N. (1981) Fracture label: cytochemistry of freeze-fracture faces in the erythrocyte membrane. *Proc. Natl. Acad. Sci. USA* **78**, 343–347.
12. Pinto Da Silva, P. and Kan, F. W. K. (1984) Label fracture: a method for high resolution labeling of cell surfaces. *J. Cell Biol.*, **99**, 1156–1161.
13. Fujimoto, K. and Ogawa, K. (1991) Fracture-flip and fracture-flip cytochemistry to study macromolecular architecture of membrane surfaces: practical procedures, interpretation and application. *Acta Histochem. Cytochem.* **24**, 111–117.
14. Fujimoto, K. and Pinto Da Silva, P. (1992) Fracture-flip/Triton X-100 reveals the cytoplasmic surface of human erythrocyte membranes. *Acta Histochem. Cytochem.* **25**, 255–263.
15. Fujimoto, K. (1997) SDS-digested freeze–fracture replica labeling electron microscopy to study the two-dimensional distribution of integral membrane proteins and phospholipids in biomembranes: practical procedure, interpretation and application. *Histochem. Cell Biol.* **107**, 87–96.
- 15a. Rash, J. E. and Yasumura, T. (1999) Direct immunogold labeling of connexins and aquaporin-4 in freeze-fracture replicas of liver, brain, and spinal cord: factors limiting quantitative analysis. *Tissue Cell Res.* **296**, 307–321.
16. Hertzberg, E. L., Anderson, D. J., Friedlander, M., and Gilula, N. B. (1982) Comparative analysis of the major polypeptides from liver gap junctions and lens fiber junctions. *J. Cell Biol.* **92**, 53–59.
17. Dunia, I., Manenti, S., Rousselet, A., and Benedetti, E. L. (1987) Electron microscopic observations of reconstituted proteoliposomes with the purified major intrinsic membrane protein of eye lens fibers. *J. Cell Biol.* **105**, 1679–1689.
18. Gong, X., Klier, G., Huang, Q., Wu, Y., Lei, H., Kumar, N. M., Horwitz, J., and Gilula, N. B. (1997) Disruption of $\alpha 3$ connexin gene leads to proteolysis and cataractogenesis in mice. *Cell* **91**, 833–843.
19. White, T. W., Bruzzone, R., Goodenough, D. A., and Paul, D. L. (1992) Mouse Cx50, a potential member of the connexin family of gap junction proteins, is the lens fiber protein MP70. *Mol. Biol. Cell.* **3**, 711–720.
20. Kistler, J., B. Kirkland, and S. Bullivant. (1985) Identification of a 70,000kD protein in lens membrane junctional domains. *J. Cell Biol.* **101**, 28–35.
21. Friedlander, M. (1980) Immunological approaches to the study of myogenesis and lens fiber junction formation. *Curr. Top. Dev. Biol.* **14**, 321–358.
22. Broekhuysse, R. M., Kuhlmann, E. D., and Stols, A. L. H. (1976) Lens membrane II. Isolation and characterization of the main intrinsic polypeptide (MIP) of bovine lens fiber membranes. *Exp. Eye Res.* **23**, 365–371.
23. Vallon, O., Dunia, I., Favard-Sereno, C., Hoebeke, J., and Benedetti, E. L. (1985) MP26 in the bovine lens: a post-embedding immunocytochemical study. *Biol. Cell* **53**, 85–88.
24. Milks, L. C., Kumar, N. M., Houghten, N., Unwin, N., and Gilula, N. B. (1988) Topology of the 32-kD liver gap junction protein determined by site-directed antibody localizations. *EMBO J.* **7**, 2967–2975.

25. Green, N., Alexander, H., Olson, A., Alexander, S., Shinnick, T. M., Sutcliffe, J. G., and Lerner, R. A. (1982) Immunogenic structure of the influenza virus hemagglutinin. *Cell* **28**, 477–487.
25. Paul, D. L., Ebihara, L., Takemoto, L. J., Swenson, K. I., and Goodenough, D. A. (1991) Connexin46, a novel lens gap junction protein, induces voltage-gated currents in nonjunctional plasma membrane of *Xenopus* oocytes. *J. Cell Biol.* **115**, 1077–1089.
26. Yeager, M. and Gilula, N. B. (1992) Membrane topology and quaternary structure of cardiac gap junction ion channels. *J. Mol. Biol.* **223**, 929–948.
27. Risek, B., Guthrie, S., Kumar, N., and Gilula, N. B. (1990) Modulation of gap junction transcript and protein expression during pregnancy in the rat. *J. Cell Biol.* **110**, 269–282.
28. Jarvis, L. J., Kumar, N. M., and Louis, C. F. (1993) The developmental expression of three mammalian lens fiber cell membrane proteins. *Invest. Ophthalmol. Vis. Sci.* **34**, 613–620.
29. Gruijters, W. T., Kistler, J., Bullivant, S., and Goodenough, D. A. (1987) Immunolocalization of MP70 in lens fiber 16–17-nm intercellular junctions. *J. Cell Biol.*, **104**, 565–572.
30. Kistler, J. and Bullivant, S. (1987) Protein processing in lens intercellular junctions: cleavage of MP70 to MP38. *Invest. Ophthalmol. Vis. Sci.* **28**, 1687–1692.
31. Li, J. S., Fitzgerald, S., Dong, Y., Knight, C., Donaldson, P., and Kistler, J. (1997) Processing of the gap junction connexin 50 in the ocular lens is accomplished by calpain. *Eur. J. Cell Biol.* **73**, 141–149.
32. Branton, D. (1966) Fracture faces of frozen membranes. *Proc. Natl. Acad. Sci. USA* **55**, 1048–1056.
33. Deamer, D. W. and Branton, D. (1967) Fracture planes in a ice-bilayer model membrane system. *Science* **158**, 655–657.
34. Pinto Da Silva, P. and Branton, D. (1970) Membrane splitting in freeze-teching: covalently bound ferritin as a membrane marker. *J. Cell Biol.* **45**, 598–604.
35. Moor, H. (1973) Cryotechnology for the structural analysis of biological material, in *Freeze-Etching, Techniques and Applications* (Benedetti, E. L. and Favard, P., eds.), French Society of Electron Microscopy, Paris, pp. 11–30.
36. Benedetti, E. L. and Favard, P. (1973) Freeze-etching, techniques and applications. French Society of Electron Microscopy, Paris, France.
37. Satir, B. H. and Satir, P. (1979) Partitioning of intramembrane particles during the freeze-fracture procedure, in *Freeze-Fracture Methods, Artifact, and Interpretations* (Rash, J. E. and Hudson, C. S., eds.), Raven Press, New York, pp. 43–49.
38. Torrisi, M. R. and Mancini, P. (1996) Freeze-fracture immunogold labeling. *Histochem. Cell Biol.*, **106**, 19–30.
39. Verkleij, J. (1984) Lipidic intramembranous particles. *Biochim. Biophys. Acta.* **779**, 43–63.
40. Hanna, R. B., Ornberg, R. L., and Reese, T. S. (1985) *Structural Details of Rapid Frozen Gap Junctions*, Cold Spring Harbor Laboratory Press, Cold Spring Harbor, New York, pp. 23–32.
41. Hirokawa, N. and Heuser, J. (1982) The inside and outside of gap-junction membranes visualized by deep etching. *Cell* **30**, 395–406.

42. Hoh, J. H., Sosinsky, G., Revel, J. P., and Hansena, P. K. (1993) Structure of the extracellular surface of the gap junction by atomic force microscopy. *Biophys. J.* **65**, 149–163.
43. Perkins, G., Goodenough, D., and Sosinsky, G. (1997) Tree-dimensional structure of the gap junction connexon. *Biophys. J.* **72**, 533–544.
44. Unger, V. M., Kumar, N. M., Gilula, N. B., and Yaeger, M. (1997) Projection structure of a gap junction membrane channel at 7 Å resolution. *Nat. Struct. Biol.* **4**, 39–43.
45. Unger, V. M., Kumar, N. M., Gilula, N. B., and Yaeger, M. (1999) Three-dimensional structure of a recombinant gap junction membrane channel. *Science* **283**, 1176–1179.
46. Foote, C. I., Zan Zhou, and Nicholson, B. J. (1998) The pattern of disulfide linkages in the extracellular loop regions of Connexin 32 suggests a model for the docking interface of gap junctions. *J. Cell Biol.* **140**, 1187–1197.
47. White, T. W., Bruzzone, R., Wolfram, S., Paul, D. L., and Goodenough, D. A. (1994) Selective interactions among the multiple connexin proteins expressed in the vertebrate lens: the second extracellular domain is a determinant of compatibility between connexins. *J. Cell Biol.* **125**, 879–892.
48. Sosinsky, G. (1996) Molecular organization of gap junction membrane channels. *J. Bioenerg. Biomembr.* **28**, 297–309.
49. Ghoshroy, R., Goodenough, D. A., and Sosinsky, E. (1995) Preparation, characterization, and structure of half gap junctional layers split with urea and EGTA. *J. Membr. Biol.* **146**, 15–28.
50. Fujimoto, K., Nagafuchi, A., Tsukita, S., Kuraoka A., Ohokuma, A., and Shibata, Y. (1997) Dynamics of connexins, E-cadherin and α -catenin on cell membrane during junction formation. *J. Cell Sci.* **110**, 311–322.
51. Furuse, M., Fujimoto, K., Sato, N., Hirase, T., Tsukita, S., and Tsukita, S. (1996) Overexpression of occludin, a tight junction-associated integral membrane protein, induces formation of intracellular multilamellar bodies bearing tight junction-structures. *J. Cell Sci.* **109**, 429–435.
52. Hirase, T., Staddon, J. M., Saitou, M., Ando-Akatsuka, Y., Itoh, M., Furuse, M., Fujimoto, K., Tsukita, S., and Rubin, L. L. (1997) Occludin as a possible determinant of tight junction permeability in endothelial cells. *J. Cell Sci.* **110**, 1603–1613.
53. Hülser, D. F., Rehkopf, B., and Traub, O. (1997) Dispersed and aggregated gap junction channels identified by immunogold labeling of freeze-fractured membranes. *Exp. Cell Res.* **233**, 240–251.
54. Fujimoto, K., Umeda, M., and Fujimoto, T. (1996) Transmembrane phospholipid distribution revealed by freeze-fracture replica labeling. *J. Cell Sci.* **109**, 2453–2460.
55. Dunia, I., Recouvreur, M., Nicolas, P., Kumar, N., Bloemendal, H., and Benedetti, E. L. (1998) Assembly of connexins and MP26 in lens fiber plasma membranes studied by SDS-fracture immunolabeling. *J. Cell Sci.* **111**, 2109–2120.
56. Benedetti, E. L., Dunia, I., Dufier, J. L., Yit K-S., and Bloemendal, H. (1996) Plasma membrane-cytoskeleton complex in the normal and cataractous lens, in *The Cytoskeleton*, Vol. 3 (Hesketh, J. E. and Pryme, I. F., eds.), JAI Press, London, pp. 451–518.

57. Deen, P. M. T. and van Os, C. H. (1998) Epithelial aquaporins *Curr. Opin. Cell Biol.* **10**, 435–442.
58. Cullen, M. J., Walsh, J., Stevenson, S. A., Rothery, S. and Severs, N. J. (1998) Co-localization of dystrophin and β -dystroglycan demonstrated in “en face” view by double-immunogold labeling of freeze-fractured skeletal muscle. *J. Histochem. Cytochem.* **46**, 945–953.
59. Nomura, R. and Fujimoto, T. (1999) Tyrosine-phosphorylated caveolin-1: immunolocalization and molecular characterization. *Mol. Biol. Cell* **10**, 975–986.
60. Reynolds, J. A. and Tandford, Ch. (1970a) The gross conformation of protein-sodium dodecyl sulfate complexes. *J. Biol. Chem.* **254**, 5161–5165.
61. Reynolds, J. A. and Tandford, Ch. (1970b) Binding of dodecyl-sulfate to proteins at high binding ratios. Possible implications for the state of proteins in biological membranes. *Proc. Natl. Acad. Sci. USA* **66**, 1002–1007.
62. Helenius, A. and Simons K. (1975) Solubilization of membranes by detergents. *Biochem. Biophys. Acta* **415**, 29–79.
63. White, F. H. and Wright, G. (1984) Effect of structure-forming solutes on chicken eggwhite lysozyme after reductive cleavage of disulfide bonds. *Int. J. Pept. Prot. Res.* **23**, 256–270.
64. Rothe, G. M. and Maurer, W. D. (1986) One dimensional PAA-gel electrophoretic techniques to separate functional and denaturated proteins, in *Gel Electrophoresis of Proteins* (Dunn, M. J., ed.), Wright Press, Bristol, UK, pp. 37–140.
65. Benedetti, E. L., and Emmelot, P. (1968) Hexagonal array of subunits in tight junctions separated from isolated rat liver plasma membranes. *J. Cell Biol.*, **38**, 15–24.
66. Dunia, I., Sen-Ghosh, K., Benedetti, E. L., Zweers, A., and Bloemendal, H. (1974) Isolation and protein pattern of eye lens fiber junctions. *FEBS Lett.* **45**, 139–144.
67. Robards, A. W. and Sleytr, V. B. (1985) Practical Methods of Electron Microscopy, in *Low Temperature Methods in Biological Electron Microscopy*, Vol. 10 (Glauert, A. M., ed.), Elsevier, Amsterdam.
68. Severs, N. J. and Shotton, D. M. (1995) Rapid freezing, freeze-fracture and deep etching, in *Techniques in Modern Biomedical Microscopy*, Wiley-Liss, New York.
69. Gross, H. (1979) Advances in ultrahigh vacuum freeze-fracturing at very low specimen temperature, in *Freeze-Fracture Methods, Artifacts and Interpretations* (Rash, J. E. and Hudson, C. S., eds.), Raven Press., New York, pp. 127–139.
70. Gulik-Krzywicki, T. (1997) Freeze-fracture transmission electron microscopy. *Curr. Opin. Colloid Interphase Sci.* **2**, 137–144.
71. Raposo, G., Kleijmeer, M., Posthuma, G., Slot, J. and Geuze, H. (1997) Immunogold labeling of ultrathin cryosections: application in immunology, in *Weir's Handbook of Experimental Immunology*, 5th ed., Vol. 4. (Herzenberg, L. A., Weir, D. and Blackwell, C., eds.), Blackwell Science, Cambridge, MA, pp. 1–11.
72. Slot J. W., Posthuma, G., Chang, L. Y., Crapo, J. D., and Geuze, H. (1989) Quantitative aspects of immunogold labeling in embedded and non-embedded sections. *Am. J. Anat.* **185**, 271–281.
73. Griffiths, G. (1993) *Fine Structure Immunocytochemistry*, Springer-Verlag, New York, New York.



<http://www.springer.com/978-0-89603-658-1>

Connexin Methods and Protocols

Bruzzone, R.; Giaume, C. (Eds.)

2001, XV, 491 p., Hardcover

ISBN: 978-0-89603-658-1

A product of Humana Press